Electronic Supplementary Material (ESI) for Journal of Materials Chemistry A.

Supporting Information for

Sub-5 nm SnO_2 Chemically Coupled Hollow Carbon Spheres for Efficient Electrocatalytic CO_2 Reduction

Yiliguma,[a] Zhijie Wang,[a] Chao Yang,[a] Anxiang Guan,[a] Longmei Shang,[a] Abdullah M. Al-Enizi,[b] Lijuan Zhang,[a] Gengfeng Zheng[a]*

[a]Laboratory of Advanced Materials, Department of Chemistry and Shanghai Key Laboratory of Molecular Catalysis and Innovative Materials, Fudan University, Shanghai 200438, China

[b]Department of Chemistry, College of Science, King Saud University, Riyadh 11451, Saudi Arabia

* Corresponding author E-mail: gfzheng@fudan.edu.cn

Table S1. Summary of our and previously reported tin oxide based catalytic CO_2RR.

Catalyst	Electrochemical CO_2RR conditions	Highest CO_2RR activity	Stability	Active sites regarding Sn oxidation states	Loading of SnO_x	Ref.
SnO_2/C	H-cell, CO_2 sat. 0.1 M $KHCO_3$ aqueous solution, pH 6.8	FE ($HCOO^-$): ~ 54% (-3.7 mA cm^{-2}), FE (CO): ~ 22% (-1.4 mA cm^{-2}) @ -0.9 V vs RHE	After 12 h @ -0.9 V vs RHE, FE ($HCOO^-$) decreased from 64% to 49%	SnO_2 (JCPDS #41-1445), SnO (JCPDS #07-0195)	SnO_2: 0.07 mg cm^{-2}	This work
Sn/SnO_x film	H-cell, CO_2 sat. 0.5 M $NaHCO_3$ aqueous solution	FE (CO): ~ 5-10% and FE (HCOOH): ~ 19% @ -0.7 V vs RHE (j_{tot} -0.4 ~ -0.6 mA cm^{-2})	/	Sn/SnO_x interface or SnO_x surface (SnO_x JCPDS # not specified)	/	S1
Hierarchical mesoporous SnO_2 Nanosheets on carbon cloth	H-cell, CO_2 sat. 0.5 M $NaHCO_3$ aqueous solution, pH 7.2	FE ($HCOO^-$): 87% @ -1.6 V vs Ag/AgCl (3 M KCl) (j_{tot} -50 mA cm^{-2})	After 24 h @ -1.6 V vs Ag/AgCl (3 M KCl) FE (HCOO-): 87%	Sn or Sn/SnO_x	SnO_2 (JCPDS #41-1445): 0.34 mg cm^{-2}	S2
SnO_2 nanoparticles on carbon aerogels	Gas diffusion electrode, H-cell, CO_2 sat. 1.0 M $KHCO_3$ aqueous solution, pH 7.5	FE ($HCOO^-$): ~76% @ -0.96 V vs RHE (j_{tot} -14 ~ -17 mA cm^{-2})	After 12 h @ -0.96 V vs RHE FE ($HCOO^-$): 66%	/	SnO_2 (JCPDS #41-1445): 0.56 mg cm^{-2}	S3
SnO_2 nanoparticles on carbon black	H-cell, CO_2 sat. 0.1 M $NaHCO_3$ aqueous solution	FE ($HCOO^-$): 86.2% @ -1.8 V vs SCE (j_{tot} -5.4 mA cm^{-2})	/	/	SnO_2 (Rutile): 0.015 mg cm^{-2}	S4
SnO_2 nanoparticles on reduced graphene oxide	H-cell, CO_2 sat. 0.1 M $NaHCO_3$ aqueous solution	FE (HCOO-): 93.6% @ -1.8 V vs SCE (j_{tot} -10.2 mA cm^{-2})	/	/	SnO_2 (Rutile): 0.015 mg cm^{-2}	S5
SnO_x / gas diffusion layer	H-cell, CO_2 sat. 0.5 M $KHCO_3$ aqueous solution	FE ($HCOO^-$): 87.1% @ -1.6 V vs SHE (j_{tot} -10 mA cm^{-2})	After 20 h @ -1.6 V vs SHE FE ($HCOO^-$): 70.2%	SnO_2 (JCPDS #46-1088), SnO (JCPDS #06-0395)	SnO_x: 3 mg cm^{-2}	S5
SnO nanoparticles on carbon	H-cell, CO_2 sat. 0.5 M $KHCO_3$ aqueous solution	FE (CO): 37% (5 mA cm^{-2}) @ -0.66 V vs RHE; FE ($HCOO^-$): ~ 65% (25 mA cm^{-2}) @ -0.86 V vs RHE	After 24 h @ -0.66 V vs RHE FE (CO): 30~40%, FE ($HCOO^-$): 36%	Ultra small Sn (JCPDS #04-0673) nanoparticles	SnO (JCPDS #06-0395): 0.14 mg cm^{-2}	S6
$Sn_6O_4(OH)_2$ nanoparticles on carbon black	Custom made cell capable of in situ AT-IR spectroscopic measurement during CO_2RR, CO_2 sat. 0.1 M K_2SO4 aqueous solution, pH 4.4	FE ($HCOO^-$): 70% @ -1.8 V vs RHE (current density not specified)	/	Sn^{2+} oxyhydroxide (JCPDS #46-1486)	$Sn_6O_4(OH)_2$: 0.57 mg cm^{-2}	S7
SnO_2 nanoparticles	Cell capable of in operando	FE ($HCOO^-$): ~80% in a	/	SnO_2 (JCPDS #41-	0.5 mg cm^{-2}	S8

on reduced graphene oxide	Raman spectroscopic study during CO_2RR, CO_2 dissolved 0.5 M NaOH, pH 9.7	potential range around from -0.9 to -1.2 V vs Ag/AgCl (3 M KCl) (j_{tot} -4.7 mA cm^{-2} @ -1.5 V vs Ag/AgCl)	1445)	(including reduced graphene oxide)

Table S2. Summary of Sn 3d, O 1s and C 1s binding energies and Sn:O atomic ratios in SnO_2/C and SnO_x hollow spheres.

		SnO_x	C	SnO_2/C
Binding Energy / eV	Sn $3d_{5/2}$	486.5	-	487.6
	O 1s	530.4	533.6	532.0
	C 1s	-	284.8	284.8
Molar Ratio	Sn:O	1:2.7	-	1:6.0
	$Sn:O_{Latt}$	1:1.0	-	1:0.16

Methods

Calculation of ratio of turnover frequencies

$$\mathrm{TOF} = \frac{J}{n \times N \times 1.602 \times 10^{-19}}$$ (*J*: catalytic current density, *n*: the numbers of electrons involved in the electrochemical reaction, *N* the areal density of active sites)[S9]

In our experiment, SnO_2/C and SnO_x are active for CO_2RR to produce formate and CO, both of which are 2 electron transfer reactions. Thus,

$$\frac{TOF_{SnO2/C}}{TOF_{SnOx}} = \frac{J_{SnO2/C} \times N_{SnOx}}{J_{SnOx} \times N_{SnO2/C}}$$

For heterogeneous catalysts, it is difficult to obtain the absolute value of N. Here, we do not consider the difference of crystalline structure between SnO_2/C and SnO_x (since they are similar) and assume SnO_2 and SnO_x nanoparticles completely cover the surface of both hollow structures. Then, the ratio of their double layer capacitances would be the ratio of their ECSA as well as ratio of the numbers of their active sites. Thus,

$$\frac{TOF_{SnO2/C}}{TOF_{SnOx}} = \frac{J_{SnO2/C} \times N_{SnOx}}{J_{SnOx} \times N_{SnO2/C}} = \frac{J_{SnO2/C} \times C_{dl\,SnOx}}{J_{SnOx} \times C_{dl\,SnO2/C}}$$

At -0.9 *mA cm*$^{-2}$ under CO_2RR condition, J_{CO2RR} for SnO_2/C and SnO_x were -5.1 and 0.19 *mA cm*$^{-2}$. Therefore,

$$\frac{TOF_{SnO2/C}}{TOF_{SnOx}} = \frac{J_{SnO2/C} \times C_{dl\,SnOx}}{J_{SnOx} \times C_{dl\,SnO2/C}} = \frac{5.1 \times 1}{0.19 \times 22} = 1.22$$

Supplementary Figures

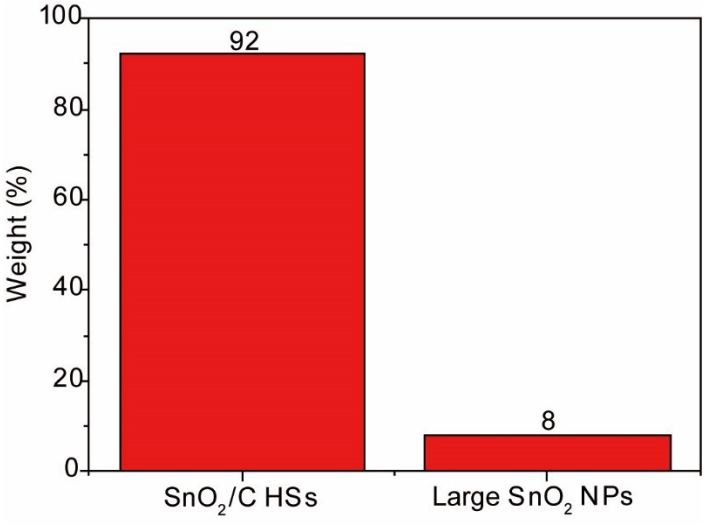

Figure S1. Estimated weight ratio of SnO_2 in SnO_2/C hollow spheres and with large particle size by XRD analysis.

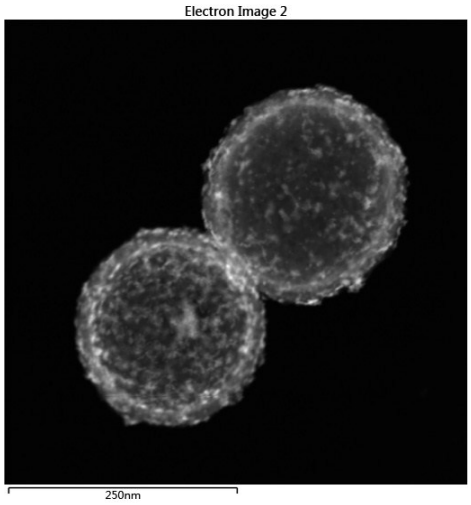

Figure S2. Dark-field STEM image of SnO_2/C hollow spheres.

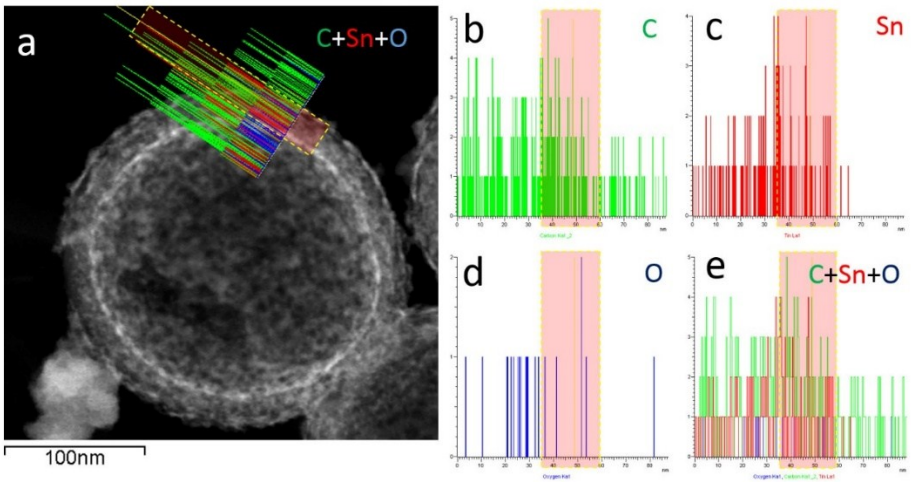

Figure S3. (a) Dark-field STEM image of one typical SnO_2/C hollow structure with the-line scan EDS across its wall. Yellow dashed rectangle area is put to highlight the elemental concentrations along direction of the wall thickness. Green (b), red (c) and blue (d) line heights indicate the concentrations of carbon, tin and oxygen elements. The superposition of the carbon, tin and oxygen signals in (e).

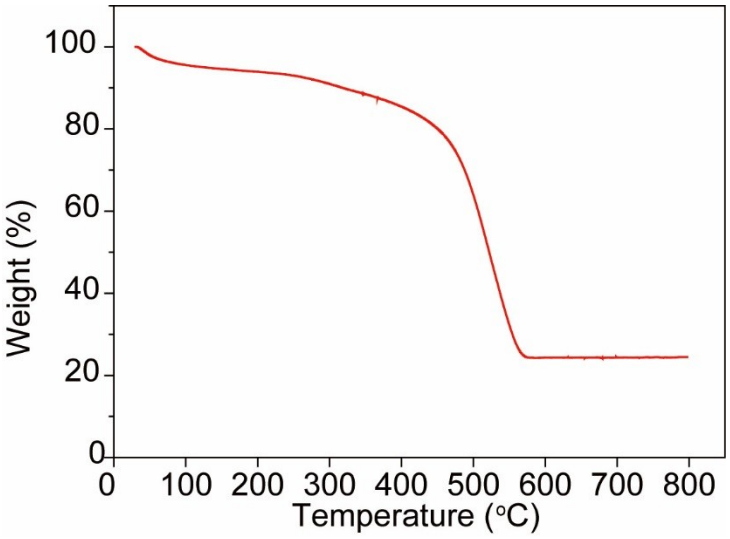

Figure S4. TGA curve of SnO_2/C hollow spheres under air with a ramp of 5 °C/min.

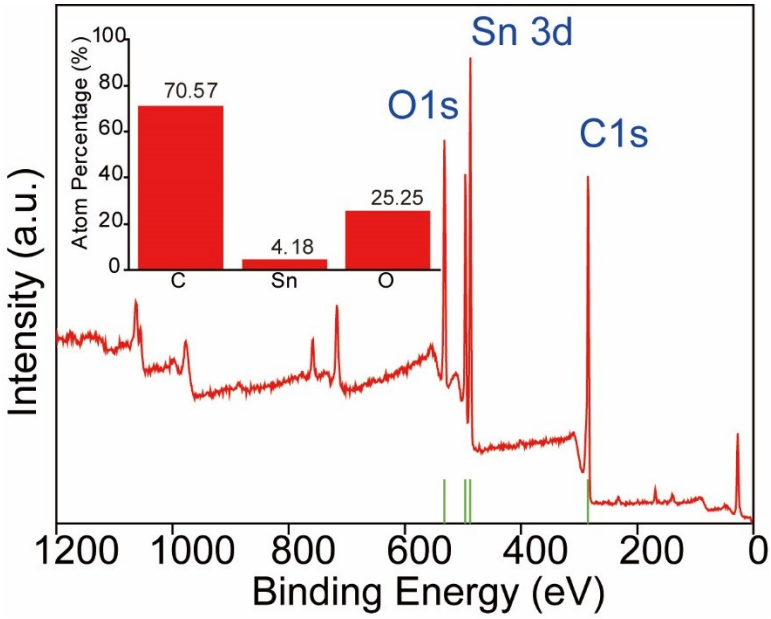

Figure S5. XPS wide spectrum of SnO_2/C hollow spheres.

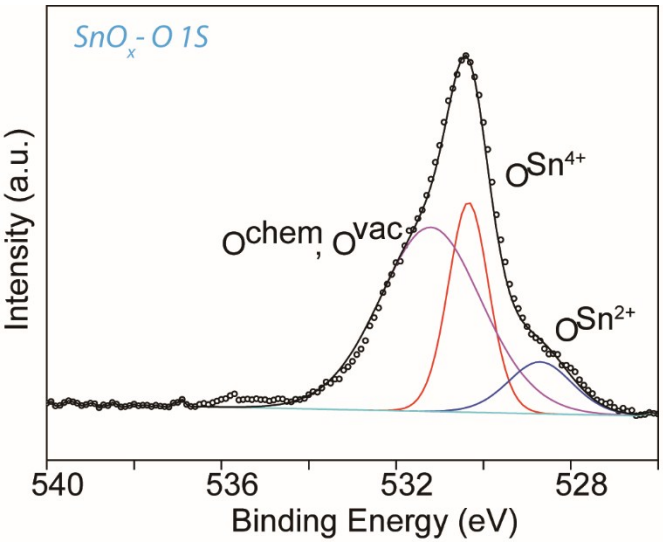

Figure S6. O 1s spectrum of SnO_x hollow spheres.

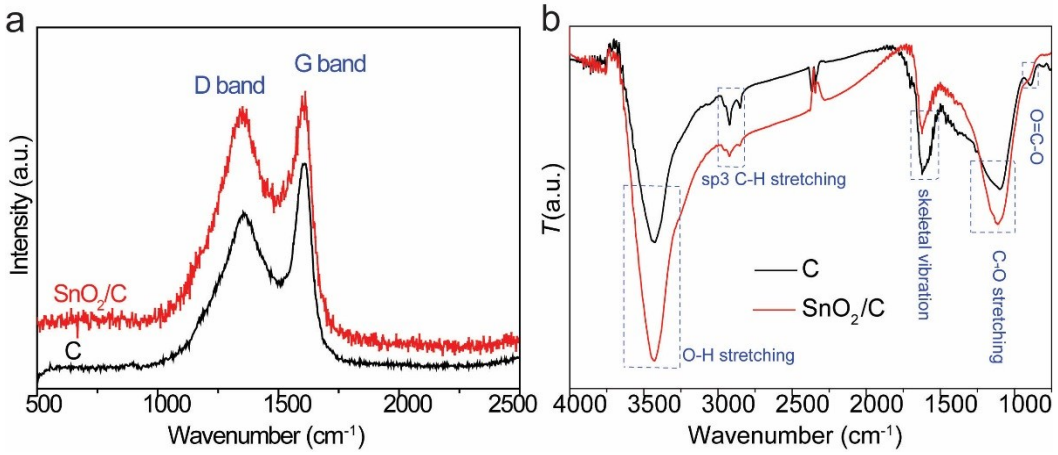

Figure S7. (a) Raman and (b) FT-IR spectra of SnO_2/C and C hollow spheres.

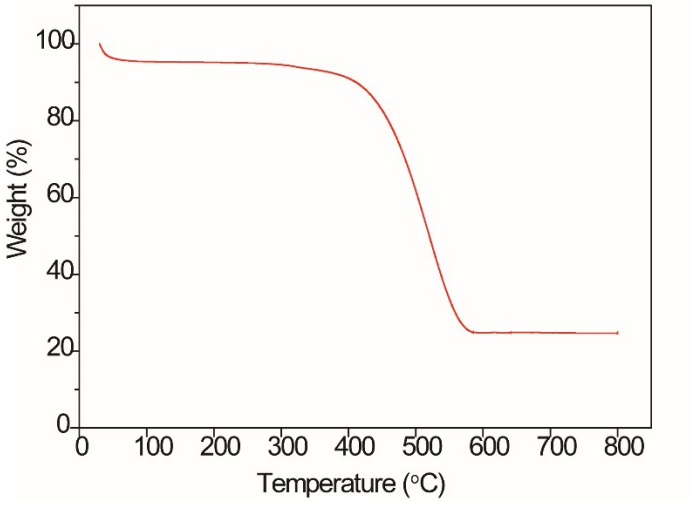

Figure S8. TGA curve of SnO_2/rGO under air with a ramp of 5 °C/min.

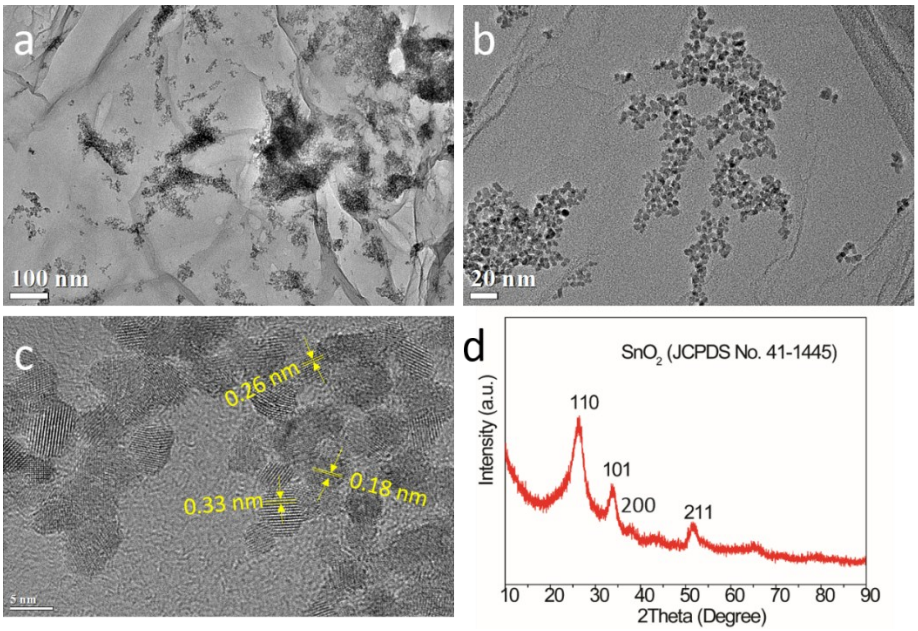

Figure S9. (a, b) TEM, (c) HRTEM and (d) XRD pattern images of SnO_2/rGO sample.

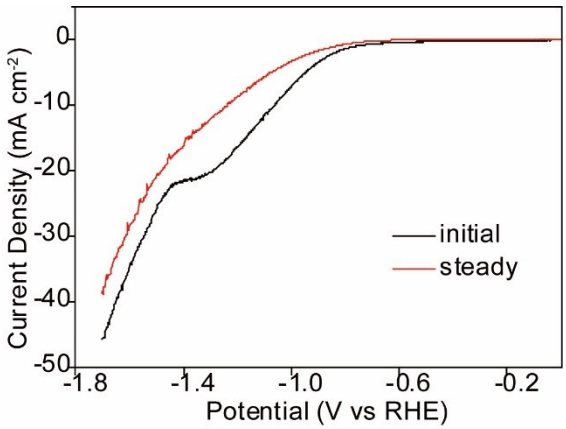

Figure S10. The first and second runs of LSV of SnO_x hollow spheres in CO_2-saturated 0.1 M $KHCO_3$ aqueous solution. The LSV curves after the second run are similar to the second one, therefore, we started CO_2RR test after the second run of LSV.

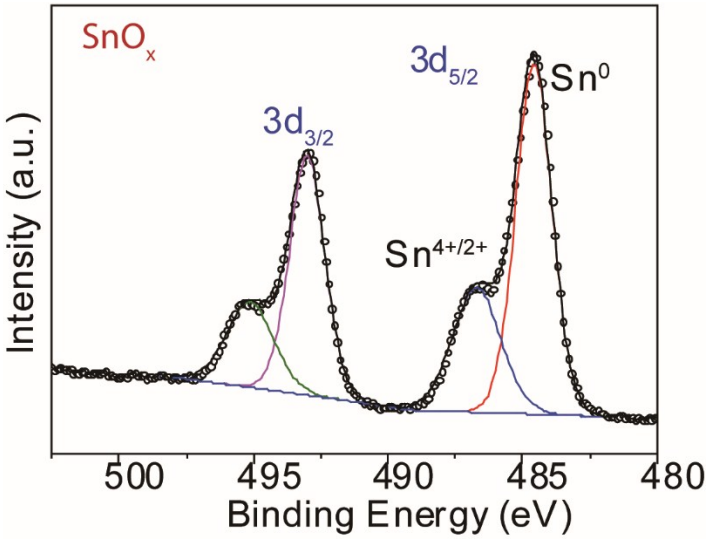

Figure S11. Sn 3d XPS spectrum of SnO_x hollow spheres after the first two runs of LSV.

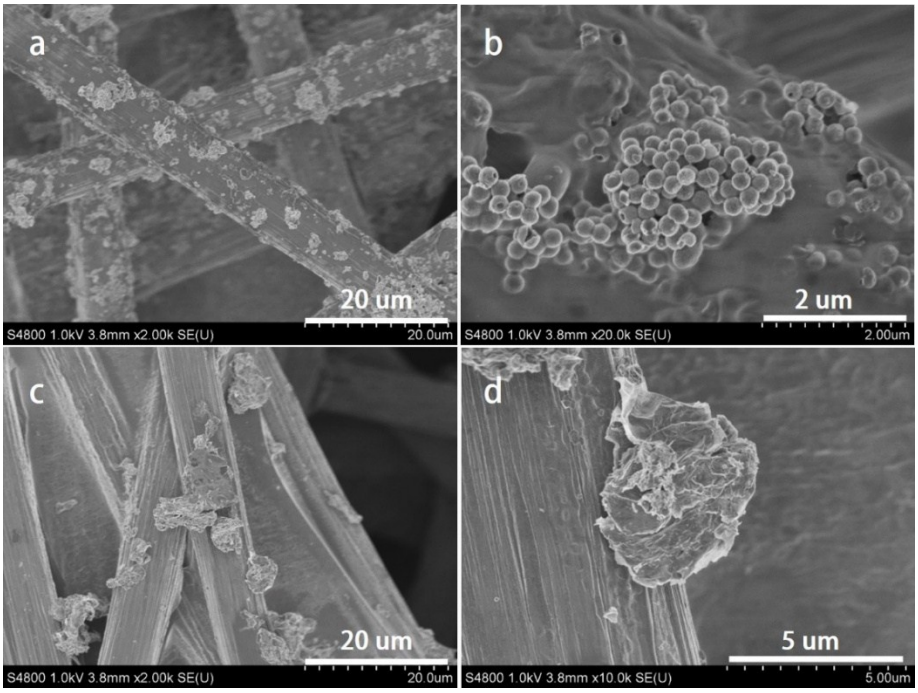

Figure S12. (a, b) SEM images of SnO_2/C hollow spheres and (c, d) SnO_2/rGO as catalysts on carbon paper electrode

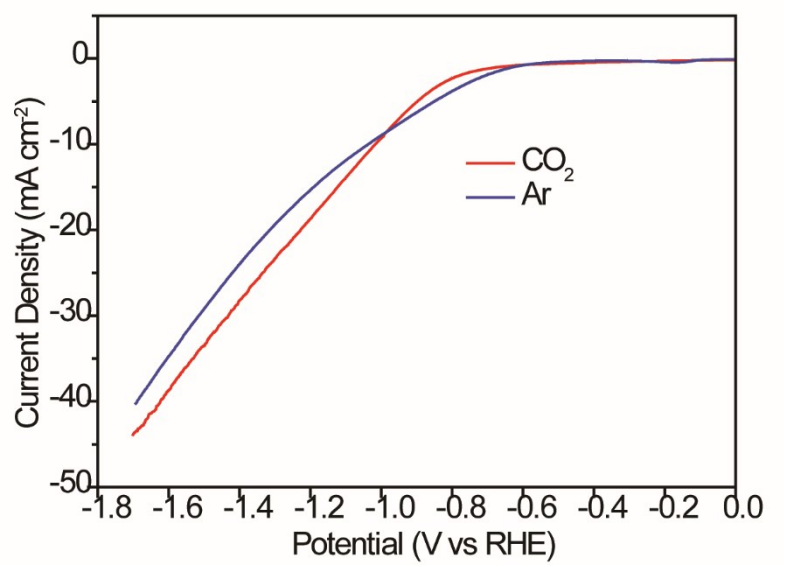

Figure S13. LSV curves of SnO_2/C in CO_2-saturated and Ar-saturated 0.1 M $KHCO_3$ aqueous solutions.

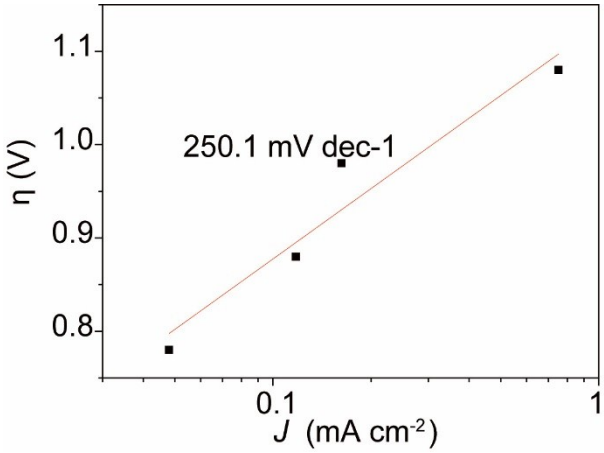

Figure S14. Tafel slope of CO_2-to-formate reaction with SnO_x hollow spheres.

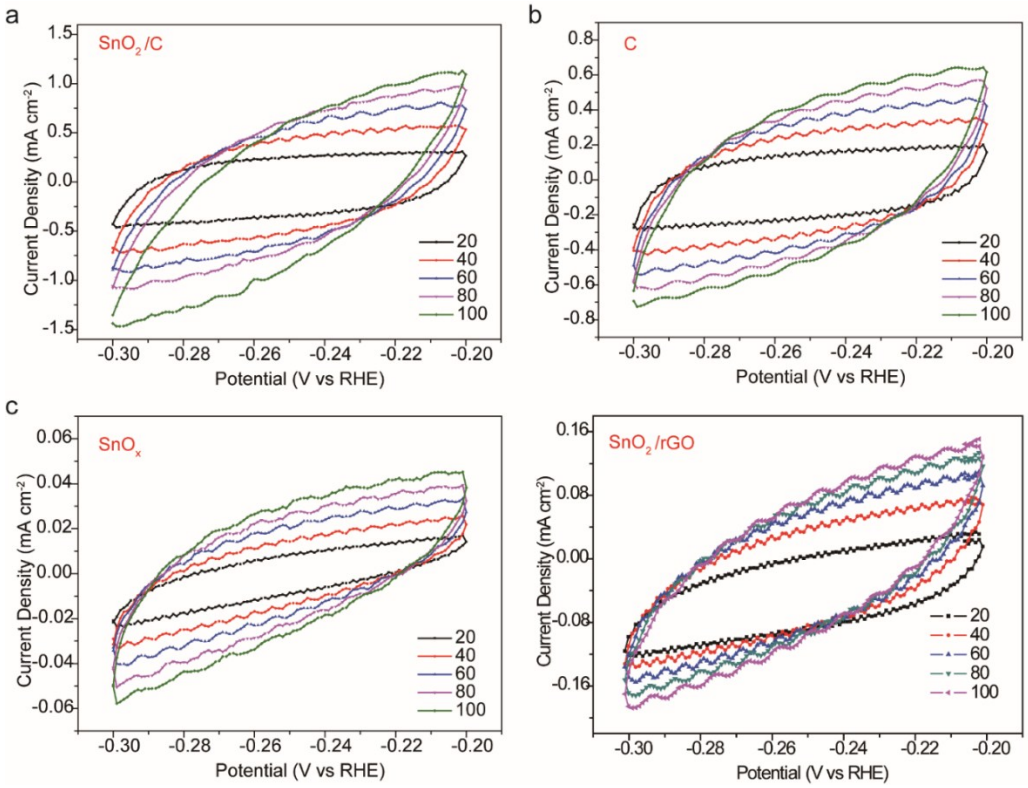

Figure S15. CV scans under different scan rates for (a) SnO_2/C, (b) C, and (c) SnO_x hollow spheres and SnO_2/rGO.

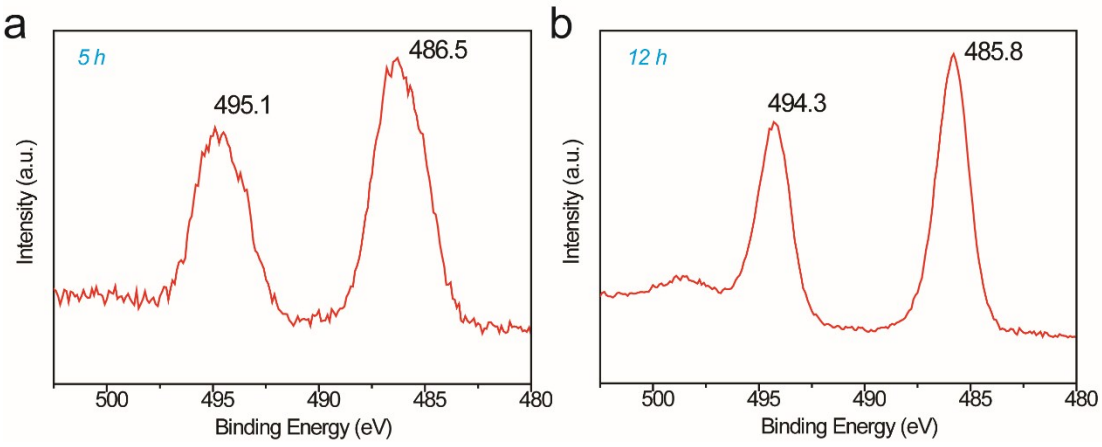

Figure S16. Sn 3d XPS spectrum of SnO_2/C hollow spheres after (a) 5 h and (b) 12 h durability test at –0.9 V vs. RHE.

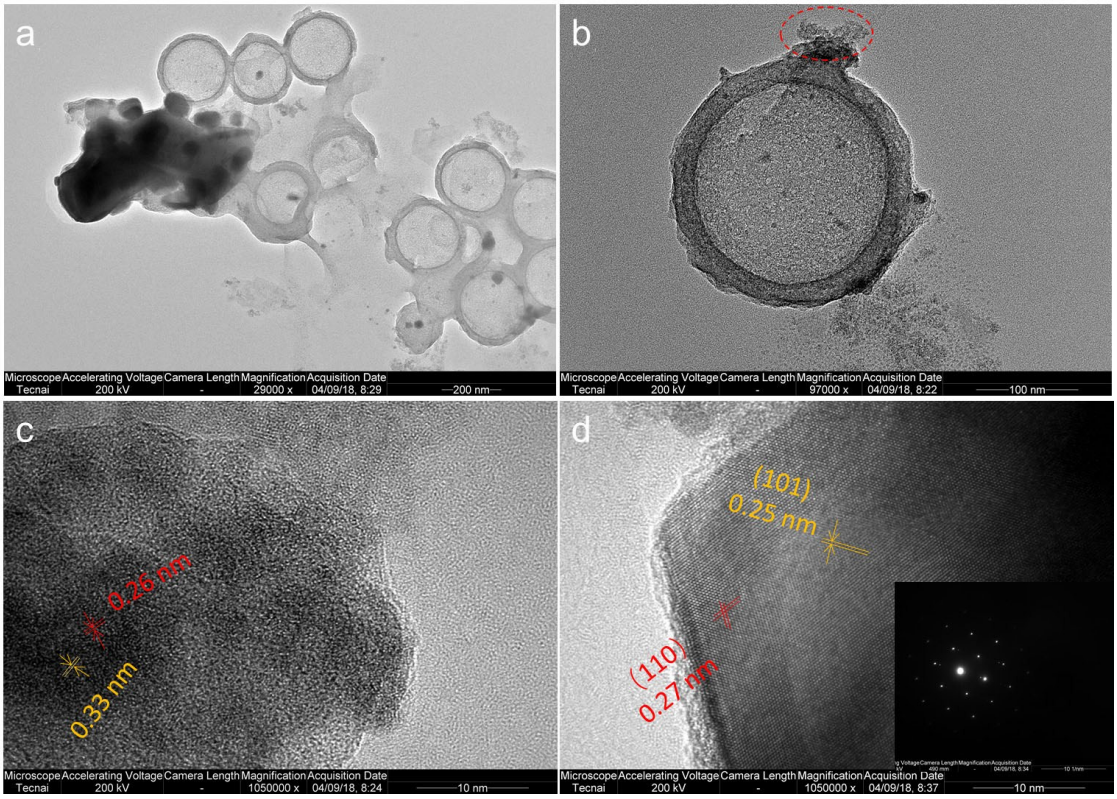

Figure S17. (a, b) TEM and (c, d) HRTEM images of SnO_2/C catalyst after 12 h durability test at –0.9 V vs RHE. In Fig. S16 a, the phase separation between carbon and Sn was observed. While the carbon hollow structure was retained after the durability test (Fig. S16a, b), the SnO_x nanoparticles agglomerated (Fig. S16b, red dashed circle, and Fig. S16c) and partial SnO_x was reduced to large size tetragonal Sn single crystals (JCPDS no. 18-1380, Fig. S16d). Under consideration of Sn 3d XPS binding energy which is closer to Sn^{2+} than Sn^{4+}, the crystal fringe distances 0.33 and 0.26 nm were assigned to SnO (JCPDS no. 07-0195) in Fig. S16c.

Reference

S1. Chen, Y.; Kanan, M. W. Tin Oxide Dependence of the CO_2 Reduction Efficiency on Tin Electrodes and Enhanced Activity for Tin/Tin Oxide Thin-Film Catalysts. *J. Am. Chem. Soc.* **2012,** *134* (4), 1986-1989.

S2. Li, F.; Chen, L.; Knowles, G. P.; MacFarlane, D. R.; Zhang, J. Hierarchical Mesoporous SnO_2 Nanosheets on Carbon Cloth: A Robust and Flexible Electrocatalyst for CO_2 Reduction with High Efficiency and Selectivity. *Angew. Chem. Int. Ed.* **2017,** *56* (2), 505-509.

S3. Yu, J.; Liu, H.; Song, S.; Wang, Y.; Tsiakaras, P. Electrochemical Reduction of Carbon Dioxide at Nanostructured SnO_2/Carbon Aerogels: The Effect of Tin Oxide Content on the Catalytic Activity and Formate Selectivity. *Appl. Catal. A: Gen.* **2017,** *545*, 159-166.

S4. Zhang, S.; Kang, P.; Meyer, T. J. Nanostructured Tin Catalysts for Selective Electrochemical Reduction of Carbon Dioxide to Formate. *J. Am. Chem. Soc.* **2014,** *136* (5), 1734-1737.

S5. Li, Y.; Qiao, J.; Zhang, X.; Lei, T.; Girma, A.; Liu, Y.; Zhang, J. Rational Design and Synthesis of SnO_x Electrocatalysts with Coralline Structure for Highly Improved Aqueous CO_2 Reduction to Formate. *ChemElectroChem* **2016,** *3* (10), 1618-1628.

S6. Gu, J.; Héroguel, F.; Luterbacher, J.; Hu, X. Densely Packed, Ultra Small SnO Nanoparticles for Enhanced Activity and Selectivity in Electrochemical CO_2 Reduction. *Angew. Chem. Int. Ed.* **2018,** *57* (11), 2943-2947.

S7. Baruch, M. F.; Pander, J. E.; White, J. L.; Bocarsly, A. B., Mechanistic Insights into the

Reduction of CO_2 on Tin Electrodes using in Situ ATR-IR Spectroscopy. *ACS Catal.* **2015,** *5* (5), 3148-3156.

S8. Dutta, A.; Kuzume, A.; Rahaman, M.; Vesztergom, S.; Broekmann, P., Monitoring the Chemical State of Catalysts for CO_2 Electroreduction: An In Operando Study. *ACS Catal.* **2015,** *5* (12), 7498-7502.

S9. Voiry, D.; Fullon, R.; Yang, J.; Silva, C. C. C.; Kappera, R.; Bozkurt, I.; Kaplan, D.; Lagos, M. J.; Batson, P. E.; Gupta, G.; Mohite, A. D.; Dong, L.; Er, D.; Shenoy, V.; Asefa, T.; Chhowalla, M., The Role of Electronic Coupling Between Substrate and 2D MoS2 Nanosheets in Electrocatalytic Production of Hydrogen. *Nature Mater.* **2016,** *15*, 1003-1010.